Published in final edited form as:

Oncogene. 2020 December ; 39(50): 7253–7264. doi:10.1038/s41388-020-01503-9.

Megalencephalic Leukoencephalopathy with Subcortical Cysts 1 (MLC1) Promotes Glioblastoma Cell Invasion in the Brain Microenvironment

John M. Lattier[†], **Arpan De**[†], **Zhihua Chen**[†], **John E. Morales**[†], **Frederick F. Lang**[†], **Jason T. Huse**[Σ], **Joseph H. McCarty**[†,*]

[†]Departments of Neurosurgery, University of Texas M. D. Anderson Cancer Center, Houston, TX

[Σ]Translational Molecular Pathology, University of Texas M. D. Anderson Cancer Center, Houston, TX

Abstract

Glioblastoma (GBM), or grade IV astrocytoma, is a malignant brain cancer that contains sub-populations of proliferative and invasive cells that coordinately drive tumor growth, progression and recurrence after therapy. Here, we have analyzed functions for megalencephalic leukoencephalopathy with subcortical cysts 1 (Mlc1), an eight-transmembrane protein normally expressed in perivascular brain astrocyte endfeet that is essential for neurovascular development and physiology, in the pathogenesis of GBM. We show that Mlc1 is expressed in human stem-like GBM cells (GSCs) and is linked to the development of primary and recurrent GBM. Genetically inhibiting MLC1 in GSCs using RNAi-mediated gene silencing results in diminished growth and invasion in vitro as well as impaired tumor initiation and progression in vivo. Biochemical assays identify the receptor tyrosine kinase Axl and its intracellular signaling effectors as important for MLC1 control of GSC invasive growth. Collectively, these data reveal key functions for MLC1 in promoting GBM cell growth and invasion, and suggest that targeting the Mlc1 protein or its associated signaling effectors may be a useful therapy for blocking tumor progression in patients with primary or recurrent brain cancer.

Keywords

cancer stem cell; Axl; Ndrg1; corpus callosum; perivascular invasion; neurovascular; angiogenesis; astrocytoma

Introduction

Glioblastoma (GBM) is a primary brain cancer that afflicts more than 10,000 adults each year in the United States [1]. Standard treatments include surgical resection followed by

[*]Corresponding Author: Joseph H. McCarty, Department of Neurosurgery, Unit 1004, University of Texas M. D. Anderson Cancer Center, 1515 Holcombe Boulevard, Houston, TX 77030, jhmccarty@mdanderson.org.

Conflict of Interest Statement: The authors have no conflicts of interest to disclose.

radiation and chemotherapy [2]. Additional targeted therapies such as bevacizumab, which inhibits intratumoral neovascularization, yield short-term benefits due to blood vessel regression and diminished blood-brain barrier (BBB) permeability; however, patients invariably develop resistance that is often associated with robust invasion [3]. Regardless of the specific treatment, GBM has a high rate of recurrence due to the presence of stem-like GBM cells (GSCs), a sub-population of cancer cells that retain invasive growth capacities [4]. GSCs often localize to specialized perivascular niches in the brain where their self-renewal and differentiation are regulated by cues from nearby stromal cells [5]. We understand surprisingly little about how GSCs preferentially thrive in the brain microenvironment to promote tumor progression or how these cells generate recurrent tumors following surgery or acquired resistance to therapy.

Mutations in the gene encoding the modulator of VRAC current 1 (MLC1) leads to the pathogenesis of megalencephalic leukoencephalopathy with subcortical cysts (MLC), a rare neurodevelopmental disease [6]. MLC is characterized by the development of perivascular astrocyte vacuolation and increased BBB permeability in brain white matter regions [7]. Mlc1 is a 38-kDa eight-transmembrane domain protein that is enriched in astrocyte end feet that closely juxtapose cerebral endothelial cells [8, 9]. Mlc1 displays sequence homology with the voltage-gated K^+ channel Kv1.1 and interacts with aquaporins, suggesting possible functions in mediating astrocyte osmoregulation [10]. Mlc1 associates with various proteins at the astrocyte surface, including Hepacam, also known as glial cell adhesion molecule (GlialCAM), a 50-kDa type one transmembrane glycoprotein [11] that is also mutated in some MLC patients [12]. Mlc1 also interacts with components of the dystrophin glycoprotein complex [13]. Although functions for Mlc1 and its interacting proteins in normal astrocytes have been described [14, 15], roles for Mlc1 in GBM cells have not been reported.

In this study we have used open source genomic database analyses combined with primary GBM cell culture systems and pre-clinical mouse models to investigate roles for MLC1 in GBM pathogenesis. We show that MLC1 mRNA and protein are highly expressed in primary human GBM in comparison to non-cancerous brain tissue, as well as robust expression in patients with recurrent tumors. RNAi-mediated inhibition of MLC1 in primary GBM cells using lentiviruses leads to reduced growth and impaired directional migration in vitro as well as diminished invasive tumor cell growth in vivo. Biochemical assays reveal that the receptor tyrosine kinase Axl and its downstream signaling effectors including Src, Erk1/2 and N-myc downstream-regulated gene-1 (Ndrg1), are differentially regulated by Mlc1 in GBM cells. Collectively, these data reveal that Mlc1 promotes GBM cell invasive growth in the brain microenvironment and suggest that targeting the Mlc1 pathway may be an effective strategy for inhibiting tumor cell invasion in patients with primary or recurrent malignant brain cancer.

Results

MLC1 is expressed in human GBM stem cells and promotes growth and self-renewal in vitro

To characterize functions for MLC1 in GBM, we first analyzed its expression in primary GSCs, which have cancer-initiating capacities and drive tumor progression and heterogeneity. The GSCs analyzed in this study have been reported to be proliferative and invasive in vivo [16, 17]. Robust levels of Mlc1 protein were detected in four of six primary human GSC spheroid samples analyzed (Figure 1A). We also analyzed Mlc1 protein expression in established GBM cell lines, including LN229, U251MG and U87MG cells, which grow as adherent cultures and are commonly used to study genes and pathways involved in malignancy and response to therapy. As shown in Figure 1B, Mlc1 protein was absent in all six GBM cell lines analyzed as determined by immunoblotting. Quantitation of MLC1 gene expression using genomic data deposited in Oncomine (oncomine.org) revealed significantly higher mRNA expression in human GSCs versus established GBM cell lines (Figure 1C). Analysis of The Cancer Genome Atlas (TCGA) database for relative levels of MLC1 mRNA in GBM versus non-cancerous brain did not reveal significant differences in expression (data not shown), likely owing to expression of Mlc1 in non-malignant astrocytes. However, TCGA analysis did reveal that MLC1 mRNA is enriched in the classical GBM sub-type (Figure 1D). This tumor sub-type is characterized by wild type TP53 status and EGFR amplification [18]. Analysis of the cBioPortal database for genes co-expressed with MLC1 revealed HEPACAM as the most correlative gene (Figure 1E), which matches with MLC1 and HEPACAM cooperative functions in neurodevelopment and the pathogenesis of MLC [12]. Additional genes with links to astroglial and glioma cell biology, including AQP4 which encodes the water channel aquaporin 4 [19] and ITGB8 which encodes the β8 integrin subunit [20, 21] show correlative expression with MLC1. Analysis of the Brain RNAseq database (brainrnaseq.org), which contains quantitative gene expression data for different fractionated neural and vascular cell types in the mouse brain, revealed that Mlc1 mRNA is highly enriched in astrocytes, similar to Aqp4 (Supplemental Figure 1A, B). Immunohistochemistry analyses of Mlc1 in the adult mouse brain confirmed expression in perivascular astrocyte end feet that juxtaposed blood vessels (Supplemental Figure 1C–E). Astrocytes cultured from mouse cerebral cortices also express Mlc1 and Aqp4 proteins, as revealed by immunoblotting detergent-soluble lysates (Supplemental Figure 1F).

To determine Mlc1 functions in GBM, we selected GSC6–27 spheroids for further mechanistic analyses. GSC6–27 cells express robust levels of Mlc1 protein (Figure 1A) and generate proliferative and invasive brain tumors after implantation in xenograft mice [22]. GSC6–27 cells were infected with pGIPZ lentiviruses expressing GFP and shRNAs targeting MLC1 (n=3). pGIPZ lentivirus expressing GFP and non-targeting shRNAs was used as a control. All three shRNAs targeting MLC1 resulted in significantly reduced protein expression as determined by immunoblotting detergent-soluble cell lysates with anti-Mlc1 antibodies (Figure 2A). Cells expressing shRNAs targeting MLC1 formed noticeably smaller spheroids (Figure 2B) that contained fewer viable cells compared to cells infected with control pGIPZ (Figure 2C). MLC1-dependent differences in cell death were not

detected as measured with cell viability assays (data not shown). Spheroid formation assays were performed to test for any MLC1-dependent difference in GBM cell proliferation and adhesion. Analysis of spheroid formation over a seven-day period revealed a reduction in proliferative capacities of GBM cells expressing MLC1 shRNAs (Figure 2D). In addition, the spheroid sizes were significantly reduced in MLC1 shRNA samples versus pGIPZ control cells (Figure 2E). At 5 days post-culturing, 25% of control neurospheres showed diameters of $<10\mu m^2$ and 65% displayed diameters of $>20\mu m^2$. In contrast, spheres that formed from cells expressing MLC1 shRNAs were predominantly smaller with 65% showing diameters of $<10\mu m^2$ (Figure 2E). Silencing MLC1 in a second primary GBM spheroid culture (GSC231) using pGIPZ lentiviral-expressed shRNAs resulted in similar defects in sphere formation and invasion through three-dimensional ECM (Supplemental Figure 2).

MLC1 is required for GBM stem cell polarity and invasion in vitro

Next, we investigated functions for Mlc1 in GSC invasion through three-dimensional ECM [23]. Spheroids were dissociated and cells were exposed to a serum gradient to induce directional invasion in an ECM-coated transwell system. In comparison to pGIPZ-infected control (NT) GBM cells, cells expressing MLC1 shRNAs showed a 75% reduction in invasion (Figure 3A). Analysis of cells that had invaded through the ECM and deposited on the underside of the transwell filter revealed differences in cell morphologies. GBM cells expressing MLC1 shRNAs displayed less polarized and elongated shapes and appeared more epithelial in comparison to cells expressing control shRNAs, which typically projected processes and were more mesenchymal in appearance (Figure 3B, C). Representative tracings of cell shape confirmed more apparent epithelial-like morphologies in cells lacking MLC1 expression, whereas cells expressing non-targeting shRNAs and Mlc1 protein appeared more polarized and mesenchymal (Figure 3C). Given the MLC1-dependent changes in GBM cell morphologies, we analyzed the expression of various protein markers involved in polarity and the epithelial to mesenchymal transition. These biomarkers include the transcription factors Snail and Slug as well as the cell adhesion and signaling proteins N-Cadherin and β-catenin. As shown in Figure 3D, elevated levels of these proteins were detected in GSCs expressing MLC1 shRNAs. In contrast, we did not detect MLC1-dependent differences in expression of vimentin, a biomarker for cells with mesenchymal-like morphologies.

MLC1 regulates intracellular signaling pathway activation in GBM stem cells

To analyze Mlc1 protein functions in promoting cell polarity leading to invasion, signaling pathways involved in adhesion and polarity were analyzed, GSC6–27 cells adhering to the ECM component laminin were immunofluorescently labeled with anti-phosphotyrosine antibodies to analyze focal adhesions. pGIPZ control expressing cells displayed polarized morphologies and extended long projections from the soma, while cells expressing MLC1 shRNAs showed less polarized morphologies and were more epithelial in appearance (Supplemental Figure 3A). Cells expressing non-targeting (NT) shRNAs averaged 90° peripheral edge angles as measured from the nucleus to the widest area of the protruding area of membrane. Cells that lacked MLC1 expression displayed edge angles of almost 270° (Supplemental Figure 3B). The intensity of anti-phosphotyrosine (pY99) immunofluorescent

signal per cell was significantly higher in cells expressing MLC1 shRNAs (Supplemental Figure 3C), possibly due to the non-polarized morphologies in these cells (Supplemental Figure 3D). MLC1 in brain astrocytes has been reported to regulate water and ion homeostasis to control cell shape and polarity [24, 25], with mutations in MLC1 leading to abnormal astroglial swelling [26–29]. However, RNA-mediated silencing of MLC1 in GSCs did not affect cell volume after exposure to hypoosmotic or hyperosmotic growth conditions (Supplemental Figure 4A). MLC1 has sequence homology to K^+ gated ion channels [10] and regulates ion flux [24]. However, K^+ ion channel activity was unaffected by silencing MLC1 in GSC6–27 cells (n=2 shRNAs) as assessed with the FluxOR Red tracer (Supplemental Figure 4B).

To determine potential Mlc1-mediated signaling functions in cells we utilized reverse-phase protein arrays (RPPA), which are antibody-based high-throughput systems to study protein signaling cascades [30] (Figure 4A). Expression of several signaling effectors involved in cell polarity and migration were down-regulated in GSC6–27 cells expressing MLC1 shRNAs in comparison to NT shRNAs (Figure 4B). These include Par-1 protein (2.1-fold lower), a scaffolding component of the cell polarity complex that has links to the cytoskeleton. The kinases Erk1/2 also showed decreased phosphorylation in cells expressing MLC1 shRNAs, indicative of diminished signaling activation. One protein showing upregulated expression in GSC6–27 cells expressing MLC1 shRNAs is the receptor tyrosine kinase Axl (6.6-fold higher) (Figure 4B). In addition, we detected increased phosphorylation of Src at the activating tyrosine 416 (Y416) as well as increased phosphorylation of Ndrg1 at pT346. Src has established roles in promoting GBM cell invasion [31], whereas Ndrg1 has reported functions in suppressing cell invasion [32]. Next , immunoblot experiments were performed to validate elevated levels of Axl protein in GSCs expressing MLC1 shRNAs. Antibodies recognizing Axl phosphorylated at amino acids Y698/Y702/Y703, which are located in the kinase domain and are phosphorylated activation, revealed increased Axl activities in cells expressing MLC1 shRNAs. (Figure 4C). The RPPA data were additionally validated by showing an MLC1-dependent increase in the phosphorylation status of Src and Ndrg1. In contrast, there was a decrease in Erk1/2 phosphorylation (Figure 4C). A complete list of proteins showing MLC1-dependent expression and/or phosphorylation by RPPA are provided in heat map (Supplemental Figure 5) and raw data formats (Supplemental Table 1).

MLC1 is required for GBM stem cell growth and invasion in xenograft mouse models

We next analyzed the functions for MLC1 in tumor initiation and progression in vivo. GSC6–27 cells infected with pGIPZ virus expressing GFP and non-targeting shRNAs (n=5) or MLC1 shRNAs (n=9) were intracranially injected into the striatum and NCR nu/nu immunocompromised mice. Animals were monitored for tumor-induced neurological deficits over a 15-week time period, and once the first animal showed deficits all mice were sacrificed. Anti-GFP antibodies were used to immunolabel fixed brain sections to monitor tumor growth patterns in the brain. pGIPZ control cells showed higher expression of Mlc1 protein as compared to cells expressing MLC1 shRNAs as revealed by immunohistochemistry (Supplemental Figure 6). Analysis of GFP expression patterns revealed few cells expressing MLC1 shRNAs in the non-injected hemisphere compared to cells expressing non-targeting shRNAs (Figure 5A–D). In addition to anti-GFP

immunostaining, a human-specific antibody recognizing vimentin (expressed by GSCs) also revealed MLC1-dependent defects in cell invasion into the opposite hemisphere (Supplemental Figure 6). Quantitation of GFP intensity from injected and non-injected hemispheres revealed MLC1-dependent cell invasion across hemispheres (Figure 5E). Myelin basic protein-expressing oligodendrocytes in white matter tracts, and particularly the corpus callosum, are a main pathway for invasion of GBM cells [33]. Tumor cells expressing control shRNAs showed robust invasion in white matter regions (Figure 5F). Cells expressing control showed distant dispersal into the non-injected hemisphere and infiltrative growth within brain tissue. In contrast, GBM cells expressing MLC1 shRNAs mostly failed to invade along the corpus callosum (Figure 5G) and showed a significant reduction in dispersal and infiltrative growth in the non-injected hemisphere (Figure 5H). Some GFP-expressing GBM cells (expressing Mlc1 shRNAs) were detected invading through the corpus callosum (Figure 5G). These cells are probably revertants that escaped MLC1 silencing in vivo. Along these lines, in mice injected with GSCs expressing MLC1 shRNAs we detect some invasive cells in the corpus callosum that express Mlc1 protein by immunohistochemistry (Supplemental Figure 6). We also detected localized MLC1-dependent defects in invasion in the brain microenvironment more proximal to the primary tumor mass (Supplemental Figure 7). Although expression of MLC1 was significantly upregulated in GBM versus non-cancerous brain, relative levels of expression were not predictive of overall patient survival (Supplemental Figure 8).

MLC1 is expressed in primary and recurrent human GBM samples

To bolster data from the xenograft mouse models of GBM, we performed immunohistochemical staining to analyze spatial patterns of Mlc1 protein expression in normal human brain and GBM tissue samples. Consistent with the mouse brain analyses showing Mlc1 mRNA expression in perivascular glial cells (Supplemental Figure 1), non-cancerous human brain tissue sections showed enriched Mlc1 protein expression in astrocytes adjacent to cerebral blood vessels (Supplemental Figure 9). Analysis of four different primary GBM samples taken from non-necrotic tumor cores revealed robust Mlc1 protein expression in cancer cells (Figure 6A–D), with enrichment in perivascular tumor cells adjacent to blood vessels. Anti-Mlc1 antibody specificity was confirmed by staining GBM sections with species-matched control IgG (Supplemental Figure 9). Analysis of the IVY-GAP database, which contains spatial characterization of gene expression from different regions of laser-dissected human GBM tissues, revealed MLC1 mRNA expression mainly within areas of invasive and infiltrative tumor growth (Supplemental Figure 10). Analysis of 11 detergent-soluble protein lysates prepared from freshly resected GBM samples by immunoblotting revealed higher Mlc1 protein expression in 8 lysates as compared to the control brain tissue sample (Figure 6E, F).

Surgery is an effective treatment for patients with GBM; however, invasive cancer cells often escape resection and contribute to tumor recurrence [33]. Given the important roles for Mlc1 in driving GBM cell invasion, we next compared Mlc1 protein expression in primary versus recurrent GBM samples (n=5 different matched patient specimens). As shown in Figure 7, Mlc1 protein was robustly expressed in cancer cells of primary tumors as well as matched recurrent tumor specimens. These data bolster roles for Mlc1 in invasive GBM cells in

driving tumor regrowth after surgery. Collectively, these various in vitro and in vivo data reveal that Mlc1 is critical for promoting invasive growth via receptor tyrosine kinase activation and regulation of intracellular signaling pathways in GBM cells (Figure 8).

Discussion

We detect MLC1-dependent GSC invasion from the main tumor mass along the entire length of the corpus callosum, with infiltrative growth of tumor cells in health brain tissue in the opposite hemisphere. While our studies have focused on GBM cell invasion through white matter, it is also likely that MLC1 facilitates perivascular GBM cell invasion. We see MLC1-dependent defects in local cell invasion from the main tumor mass, indicating defects in blood vessel interactions. Indeed, a developmental function for the Mlc1 protein in perivascular astrocytes is to control contact and communication with endothelial cells in the neurovascular unit [9].

Given that MLC1 is involved in promoting astrocyte polarity and communication with nearby cell types in the healthy brain [25], we propose that loss of Mlc1 protein expression in cells negatively impacts their mesenchymal morphologies, thus impairing their interactions with adjacent stroma and invasive capacities. Along these lines, we detected MLC1-dependent cell invasion defects in vitro accompanied with a loss of polarity and a more epithelial-like cell morphology that was unlike the mesenchymal morphology normally seen in MLC1-expressing GBM cells. Analysis of adherent cultures further revealed that cells lacking Mlc1 protein expression displayed non-polarized and epithelial-like morphologies as compared to the elongated, directional leading edge seen in control cells. In addition, spheroid formation was significantly inhibited after RNAi-mediated silencing of MLC1, suggesting that Mlc1 is necessary for maintaining proper cell-cell interactions typical of stem-like cancer cells. The RPPA analyses of GSCs revealed MLC1 regulation of signaling proteins involved in invasive cell growth. For example, PAR is a scaffolding component and component of the cell polarity complex [34] that is down-regulated in cells that lack MLC1 expression. In contrast, the Axl receptor tyrosine kinase is upregulated and hyperactivated in GBM cells expressing MLC1 shRNAs. A prior report has shown that Axl is broadly expressed in GBM where it has cancer cell-intrinsic functions involved in cell polarity and is also involved in recruiting immune cells to the tumor microenvironment [35, 36]. Activation of Axl following binding to its Gas6 ligand stimulates the phosphorylation of Src [37] and Ndgr1 in ovarian cancer cells [38], which is consistent with our data showing Mlc1-dependent links between Axl, Src and Ndrg1 in GBM cells. A prior report has linked MLC1 to the expression levels of another receptor tyrosine kinase, EGFR, in cultured astrocytes [39]. MLC1 has more recently been linked to EGFR signaling in low-grade human gliomas harboring R132H mutations in the IDH1 gene [40]. Hence, it is enticing to speculate the loss of MLC1 in GBM cells causes an imbalance in receptor tyrosine kinase expression and/or signaling, leading to a transition from a mesenchymal to an epithelial-like morphology with diminished growth and invasion. We also speculate that loss of MLC1 expression leads to impaired GSC invasion due to defective intracellular signaling involving the Erk1/2 pathway, which is less active in MLC1 shRNA cells. In ovarian cancer cells Axl signaling leads to reduced Erk1/2 phosphorylation and this correlates with a more epithelial-like cell state due to higher activities of the phosphatase DUSP4 [41]. MLC1 in astrocytes

has also been reported to inhibit Erk1/2 signaling via connexins involved in direct cell-cell communication [42]. In addition, we have shown that the metastasis suppressor Ndrg1 is hyperphosphorylated in GSCs expressing MLC1 shRNAs, revealing that multiple pathways downstream of Mlc1 likely promote GBM cell polarity and invasion. Interestingly, even though MLC1-silenced GSCs are more epithelial in morphology, we have found that many proteins with links to the mesenchymal cell state such as Snail, Slug, and N-cadherin, are actually upregulated. This suggests that loss of MLC1 expression after RNAi-mediated silencing may impact the differentiation status of GSCs. Alternatively, upregulation of proteins involved in epithelial to mesenchymal transition could be a compensatory mechanism used by GSCs when Mlc1-regulated signaling components that drive invasion are not sufficiently expressed or activated. It will be important to fully characterize Mlc1-dependent pro-invasive signaling events to determine which if these pathways can be targeted to more effectively block GBM cell invasive growth.

The levels of MLC1 expression were variable among the different GSC cultures we analyzed, with some GSCs lacking detectable levels of endogenous expression. We attempted to forcibly express MLC1 in a GSC spheroid culture that lacks endogenous MLC1 (GSC11 cells), but we found that most infected cells did not survive and cells that did survive lacked MLC1 expression (unpublished data). It will be interesting to determine what mechanisms GSCs utilize to compensate for lack of endogenous MLC1 expression as well as why forced expression of MLC1 in these cells leads to reduced viability. From studies of patients with MLC disease, the physiological functions for Mlc1 protein involves the regulation of water and ion homeostasis and cell volume control in astrocytes and other glial cell types [43]. Both osmotic stress and K^+ channel transport assays did not yield significant results pertaining to MLC1 functions. Expression of other ion channels and possibly other regulatory proteins with functions similar to Mlc1 could account for the lack of differences in ion flux [44]. Mlc1 also regulates chloride channel conductance [45], and it will be important to determine if tumor cells that lack Mlc1 have defects in this pathway. It will also be important to identify regulatory pathways that control MCL1 gene expression in GSCs, since these pathways are likely defective in GBM cell lines. We discovered through analysis of the cBioPortal database that expression of MLC1 tightly correlates with expression of ITGB8, which encodes β8 integrin. Integrin αvβ8 is a receptor for latent TGFβs in the ECM and activates TGFβ signaling events via Smad transcription factors [46]. Analysis of the MLC1 promoter sequence reveals conserved Smad-binding elements: tcgggCTCCag for MLC1 (data not shown). It will be interesting to determine if αvβ8 integrin-mediated TGFβ activation and signaling via Smads promotes MLC1 gene expression. It is also possible that integrin-mediated TGFβ activation may regulate Mlc1 protein stability at the GSC plasma membrane.

A central conclusion from this study is that MLC1 is involved in regulating cell shape and polarity, thus enabling GBM cells to navigate through the complex brain milieu. In conjunction with Mlc1, other interacting proteins such as GlialCAM are likely involved in promoting GSC polarity and invasion. In astrocytes, post-translational trafficking of Mlc1 from the endoplasmic reticulum to the cell membrane is dependent upon interactions with GlialCAM [47]. Mlc1/GlialCAM interact with Aqp4 and Trpv4, both components of the dystrophin-glycoprotein complex in astrocytes which also includes the intracellular adapter

proteins α-dystrobrevin and dystrophin, α/β-dystroglycan transmembrane proteins, and matrix proteins such as agrin, laminin, and integrin adhesion. receptors [13, 48]. Interestingly, our gene correlation analyses reveal that DTNA, which encodes α-dystrobrevin, is co-expressed with MLC1. The dystrophin-glycoprotein complex is enriched at the astrocyte-blood vessel interface [49] and has important but understudied roles in regulating BBB development and integrity. Functions for Mlc1 and its links to GlialCAM and the DGC in malignant brain tumors remains largely unknown and will be an important area of future investigation.

Materials and Methods

Human GBM cells and immunohistochemistry

Approval for the use of human specimens was obtained from the Institutional Review Board (IRB) at the University of Texas MD Anderson Cancer Center. The IRB waived the requirement for informed consent for previously collected residual tissues from surgical procedures stripped of unique patient identifiers according to the Declaration of Helsinki guidelines. GSC11, GSC13, GSC23, GSC6–27, GSC8–11, and GSC231 cells were cultured from freshly resected human tumors and have been described elsewhere [20]. GSCs were grown in DMEM Ham's F12 50/50 medium with L-glutamine (Corning, 10–090-CV) with 1X B27 supplement (Life Technologies, 17504–044), 20 ng/mL EGF (Biosource, PHG0313), 20 ng/mL bFGF (Biosource, PHG0021), and 1X Penicillin-Streptomycin (Gibco, 15140–122). GSCs formed neurosphere-like spheroids *in vitro* and were dissociated using 50 μL Accutase (Sigma, A6964) per 1×10^6 cells. GSCs were made adherent by withdrawing EGF/FGF from the growth medium and culturing on glass slips coated with poly-L-ornithine (1:100;Sigma, P4957) and laminin (1:300; Sigma, L2020) from Engelbreth-Holm-Swarm murine sarcoma basement membrane. Genomic validation of GSCs was performed by DNA short tandem repeat profiling in a CCSG-funded Characterized Cell Line Core Facility. GSCs were routinely tested for mycoplasma using commercially available kits (Thermo Fisher), and only those cells deemed mycoplasma-free were used for experiments.

GSCs were centrifuged at 1000 RPM and pellets were washed with phosphate buffered saline (PBS) and lysed using either radioimmunoprecipitation assay buffer (RIPA: 50 mM Tris-HCl pH 8.0, 150 mM NaCl, 1% sodium deoxycholate, 1% Triton X-100, 0.1% SDS, 1 mM EDTA) or NP-40 for immunoprecipitation (50 mM Tris-HCl pH 8.0, 150 mM NaCl, 1% NP-40) with protease and phosphatase inhibitors (Roche). Protein concentrations were determined using bicinchonic acid assay (BCA, Thermo Scientific). For western blot analysis, SDS-PAGE were performed with 10% polyacrylamide gels, transferred to nitrocellulose membranes (Bio-Rad), blocked using Odyssey blocking buffer (LI-COR), and incubated with specific primary antibodies diluted in blocking buffer. Secondary antibodies (IRDye 800CW goat anti-rabbit and IRDye 680RD goat anti-mouse) were purchased from LI-COR and used at 1:15,000 dilution. Western blots were finally scanned using the Odyssey CLx infrared imaging system with Image Studio (LI-COR).

Human GBM lysates, tissue sections and normal human brain tissue were acquired from the Department of Neurosurgery at The University of Texas M.D. Anderson Cancer Center in

accordance with the IRB as stated previously. For all immunohistochemistry, permeabilization was performed with 0.1% PBS-Tween, antigen retrieval was performed using 10 mM Tris-HCl pH 9.0, 1 mM EDTA, and 0.05% Tween-20, and slide sections were blocked with species-specific serum matching the secondary antibody host (Dako) and developed using ImmPACT DAB purchased from Vector (SK-4105). For all immunofluorescence, slide sections were permeabilized in 0.2% Triton X-100 in PBS, blocked with 1% BSA in permeabilization buffer, and probed with secondary antibodies from Jackson ImmunoResearch were used.

Cell invasion assays

Matrigel chambers were purchased from Corning (354480). The upper chamber was seeded with 5×10^4 GSCs in DMEM Ham's F12 medium with B27 supplement, EGF, and FGF (GSC medium). The lower chamber was filled with DMEM Ham's F12 medium containing only 10% fetal bovine serum used as a chemoattractant. All media contained 1X Penicillin-Streptomycin. Cells were incubated at 37°C with 5% CO_2 for 24 hours. Non-invading cells were removed by vigorous cotton swabbing. The remaining cells were fixed in 4% paraformaldehyde and stained with hematoxylin. GSC response to osmotic stress was tested by growing cells in GSC media containing 60 mM, 120 mM, or 220 mM NaCl where DMEM Ham's F12 media were diluted (1:1) using various concentrations of NaCl in sterile water to adjust the final concentrations . B27 supplement, EGF, and bFGF were added to the final volume. Neurospheres were grown for 7 days, cells were dissociated, and cell volume and viability were analyzed using the Beckman Coulter Vi-Cell Auto cell viability analyzer (n=4 technical replicates, with n=4 biological replicates per sample). K^+ activity was measured with the FluxOR Red K^+ Channel Assay purchased from Invitrogen (F20018). GSC6–27 cells were plated at a concentration of 2×10^5 cells/mL on black 96-well plates coated with poly-L-ornithine and laminin as described above. Cells were loaded with FluxOR Red reagent for 1 hour at 37°C, stimulated with the thallium-based High K^+ Stimulus Buffer for voltage-gated K^+ channels, according to manufacturer's protocols, and read using the Synergy 4 plate reader (BioTek Instruments) with standard TRITC filters. Multi-channel pipettes were used to dispense all volumes.

Plasmids and lentiviral vectors

GSC6–27 were infected overnight with concentrated pGIPZ lentivirus at a multiplicity of infection of 1.0. The following clones were used for MLC1 shRNA: V3LHS_320474, V3LHS_320475, V3LHS_320477, and V2LHS_87221 versus control pGIPZ containing RFP (GE Dharmacon). HEK293T were transfected with MLC1 ORF using the Precision LentiORF (pLOC) vector PLOHS_100000173 versus control pLOC (GE Dharmacon). All HEK293T were transfected overnight using Lipofectamine 3000 (Thermo Fisher).

Antibodies

A complete list of commercially available primary and secondary antibodies used in this study is provided in Supplemental Table 2. Rabbit anti-MLC1 antibody used for western blot (1:500) and immunochemistry (1:100) was purchased from Novus Biologicals (NBP1–81555). Human-specific goat anti-Vimentin was used for immunohistochemistry (1:40) and was purchased from R&D (AF2105). Rabbit anti-phosphotyrosine pY99 was used for

immunofluorescence (1:50) and was purchased from Santa Cruz (sc-7020). Rabbit anti-myelin basic protein (MBP) was used for immunofluorescence (1:200) and was purchased from Abcam (ab40390). Chicken anti-GFP was used for immunofluorescence (1:1000) and was purchased from Aves (GFP-1020). Mouse anti-Myc antibody was used for immunoprecipitation (1μg per 2mg lysate) and western blot (1:2000) and was purchased from Invitrogen (46–0603). Mouse anti-α-Actinin antibody was used for western blot (1:2000) and was purchased from Abcam (ab18061). Mouse anti-GAPDH was used for western blot (1:2000) and was purchased from Sigma (G8796).

Xenograft mouse models of GBM

Mouse studies were reviewed and approved prior to experimentation under the guidelines of the Institutional Animal Care and Use Committee and The University of Texas M.D. Anderson Subcommittee on Animal Studies, both AAALAC accredited institutions. Male nude (NCR nu/nu) mice were purchased from Jackson Laboratories and used for all GSC implantation experiments. Randomization was not used since all mice used were the same age and sex. Seven-week-old mice were anesthetized and a needle was used to dispense 1.5×10^5 pGIPZ-infected GSC6–27 cells through an intracranially inserted guide screw. GSCs expressing control shRNAs (n=5 mice) and MLC1 shRNAs (n=9 mice) were used for subsequent analyses. The sample size was selected to ensure power analyses using $\alpha = 0.05$ and an effect size = 0.4 for comparing the two groups using one-way ANOVA. There was similar variance between the control NT shRNA and MLC1 shRNA experimental groups. Mice were euthanized at 15 weeks post-injection, perfused with 4% PFA/PBS and brains were sectioned for experimental analyses. Animals were excluded from the analysis if death occurred before 15 weeks post-injection.

Reverse phase protein arrays

Adherent cells were washed twice in ice-cold PBS, then lysed in RIPA buffer or RPPA lysis buffer containing 1% Triton X-100, 50 mM Hepes pH 7.4, 150 mM NaCl, 1.5 mM $MgCl_2$, 1 mM EGTA, 100 mM NaF, 10 mM sodium pyruvate, 1 mM Na_3VO_4, 10% glycerol, and a cocktail of protease and phosphatase inhibitors (Roche Diagnostics, Mannheim, Germany) for 20 to 30 minutes with frequent mixing on ice, then were centrifuged at 14,000 RPM at 4°C for 15 minutes to isolate the detergent-soluble protein supernatant. The protein concentration was determined using the BCA Assay (or Bradford), the optimal protein concentration of lysates for RPPA is about 1.2 μg/μl (1.2 mg/ml). Lysates were denatured in 4 × SDS/2-ME sample buffer (35% glycerol, 8% SDS, 0.25 M Tris-HCl, pH 6.8; (no β-mercaptoethanol) for 5 minutes at 95°C. Lysates were stored at −80°C and subsequently analyzed in the RPPA core facility at MD Anderson Cancer Center. Samples were serially diluted and probed with 447 antibodies and arrayed on nitrocellulose-coated slides. Relative protein levels were normalized for protein loading and determined by interpolation of each dilution curve from the standard curve. Normalized data points were transformed to a linear value used for analysis.

Quantitation and statistical analysis

Brain sections were imaged using Olympus IX81 FLUOVIEW FV1000 confocal laser scanning microscope. Zeiss AxioImager Z1 fluorescence microscope was used for cell

immunofluorescence , and bright field microscopy was performed using the Zeiss AxioVert 200 camera (Carl Zeiss Microscopy). Photoshop (Adobe) was used for image compilation. Graphical representation of data and all statistical analyses was performed using GraphPad Prism. Data were presented as mean with standard deviation unless otherwise noted. Differences between groups were analyzed using two-way analysis of variance (ANOVA) with Bonferroni post-hoc test and with the following denotations for statistical significance: *p<0.05, **p<0.01, ***p<0.001, ****p<0.0001. Brain tumor sections from NT shRNA and MLC1 shRNA groups were de-identified prior to analysis and the investigators were blinded to the sample identities.

Dissociated cells were counted using a hemocytometer and non-viable cells were excluded from cell number quantitation. ImageJ (NIH.gov), was used for quantifying neurosphere size by measuring the diameter of individual neurospheres. Leading edges and cell shapes were traced manually, and cell circularity was calculated by the following equation: circularity = $4\pi(\text{area}/\text{perimeter})^2$. Anti-GFP and anti-phosphotyrosine signals were also calculated in ImageJ by converting color images to single channels and quantifying signal intensity normalized to background intensity. Cell volume in response to osmotic stress was quantified by Beckman Coulter Vi-Cell Auto. Matrigel invasion was calculated by counting the total number of cells that invaded through Matrigel pores to the opposite side of the well in a bright field microscope.

Supplementary Material

Refer to Web version on PubMed Central for supplementary material.

Acknowledgements

We thank the various members of the McCarty laboratory for insightful comments on the manuscript. This work was supported, in part, by grants to J. H. M. from the Cancer Prevention and Research Institute of Texas (RP180220), the National Institutes of Health (R01NS087635, R21NS103841, P50CA127001), the Brockman Foundation, and the Terry L. Chandler Foundation. The following NCI-funded Cancer Center Support Grant (CCSG) Core Facilities were instrumental in data acquisition: the shRNA and ORFeome Core, the Research Histopathology Facility, the Flow Cytometry and Cellular Imaging Facility, and the Sequencing and Microarray Facility.

References

1. Wen PY, Weller M, Lee EQ, Alexander BA, Barnholtz-Sloan JS, Barthel FP et al. Glioblastoma in Adults: A Society for Neuro-Oncology (SNO) and European Society of Neuro-Oncology (EANO) Consensus Review on Current Management and Future Directions. Neuro Oncol 2020.
2. Muir M, Gopakumar S, Traylor J, Lee S, Rao G. Glioblastoma multiforme: novel therapeutic targets. Expert Opin Ther Targets 2020: 1–10.
3. Garcia J, Hurwitz HI, Sandler AB, Miles D, Coleman RL, Deurloo R et al. Bevacizumab (Avastin(R)) in cancer treatment: A review of 15 years of clinical experience and future outlook. Cancer Treat Rev 2020; 86: 102017. [PubMed: 32335505]
4. Lathia JD, Mack SC, Mulkearns-Hubert EE, Valentim CL, Rich JN. Cancer stem cells in glioblastoma. Genes Dev 2015; 29: 1203–1217. [PubMed: 26109046]
5. Jhaveri N, Chen TC, Hofman FM. Tumor vasculature and glioma stem cells: Contributions to glioma progression. Cancer letters 2016; 380: 545–551. [PubMed: 25527451]

6. van der Knaap MS, Boor I, Estevez R. Megalencephalic leukoencephalopathy with subcortical cysts: chronic white matter oedema due to a defect in brain ion and water homoeostasis. Lancet Neurol 2012; 11: 973–985. [PubMed: 23079554]
7. Lopez-Hernandez T, Sirisi S, Capdevila-Nortes X, Montolio M, Fernandez-Duenas V, Scheper GC et al. Molecular mechanisms of MLC1 and GLIALCAM mutations in megalencephalic leukoencephalopathy with subcortical cysts. Hum Mol Genet 2011; 20: 3266–3277. [PubMed: 21624973]
8. Boor I, Nagtegaal M, Kamphorst W, van der Valk P, Pronk JC, van Horssen J et al. MLC1 is associated with the dystrophin-glycoprotein complex at astrocytic endfeet. Acta Neuropathol 2007; 114: 403–410. [PubMed: 17628813]
9. Boor PK, de Groot K, Waisfisz Q, Kamphorst W, Oudejans CB, Powers JM et al. MLC1: a novel protein in distal astroglial processes. J Neuropathol Exp Neurol 2005; 64: 412–419. [PubMed: 15892299]
10. Lanciotti A, Brignone MS, Molinari P, Visentin S, De Nuccio C, Macchia G et al. Megalencephalic leukoencephalopathy with subcortical cysts protein 1 functionally cooperates with the TRPV4 cation channel to activate the response of astrocytes to osmotic stress: dysregulation by pathological mutations. Hum Mol Genet 2012; 21: 2166–2180. [PubMed: 22328087]
11. Jeworutzki E, Lopez-Hernandez T, Capdevila-Nortes X, Sirisi S, Bengtsson L, Montolio M et al. GlialCAM, a protein defective in a leukodystrophy, serves as a ClC-2 Cl(−) channel auxiliary subunit. Neuron 2012; 73: 951–961. [PubMed: 22405205]
12. Lopez-Hernandez T, Ridder MC, Montolio M, Capdevila-Nortes X, Polder E, Sirisi S et al. Mutant GlialCAM causes megalencephalic leukoencephalopathy with subcortical cysts, benign familial macrocephaly, and macrocephaly with retardation and autism. American journal of human genetics 2011; 88: 422–432. [PubMed: 21419380]
13. Ambrosini E, Serafini B, Lanciotti A, Tosini F, Scialpi F, Psaila R et al. Biochemical characterization of MLC1 protein in astrocytes and its association with the dystrophin-glycoprotein complex. Mol Cell Neurosci 2008; 37: 480–493. [PubMed: 18165104]
14. Capdevila-Nortes X, Jeworutzki E, Elorza-Vidal X, Barrallo-Gimeno A, Pusch M, Estevez R. Structural determinants of interaction, trafficking and function in the ClC-2/MLC1 subunit GlialCAM involved in leukodystrophy. J Physiol 2015; 593: 4165–4180. [PubMed: 26033718]
15. Gilbert A, Vidal XE, Estevez R, Cohen-Salmon M, Boulay AC. Postnatal development of the astrocyte perivascular MLC1/GlialCAM complex defines a temporal window for the gliovascular unit maturation. Brain Struct Funct 2019; 224: 1267–1278. [PubMed: 30684007]
16. Balasubramaniyan V, Vaillant B, Wang S, Gumin J, Butalid ME, Sai K et al. Aberrant mesenchymal differentiation of glioma stem-like cells: implications for therapeutic targeting. Oncotarget 2015; 6: 31007–31017. [PubMed: 26307681]
17. Minata M, Audia A, Shi J, Lu S, Bernstock J, Pavlyukov MS et al. Phenotypic Plasticity of Invasive Edge Glioma Stem-like Cells in Response to Ionizing Radiation. Cell Rep 2019; 26: 1893–1905 e1897. [PubMed: 30759398]
18. Verhaak RG, Hoadley KA, Purdom E, Wang V, Qi Y, Wilkerson MD et al. Integrated genomic analysis identifies clinically relevant subtypes of glioblastoma characterized by abnormalities in PDGFRA, IDH1, EGFR, and NF1. Cancer cell 2010; 17: 98–110. [PubMed: 20129251]
19. Amiry-Moghaddam M AQP4 and the Fate of Gliomas. Cancer Res 2019; 79: 2810–2811. [PubMed: 31160309]
20. Guerrero PA, Tchaicha JH, Chen Z, Morales JE, McCarty N, Wang Q et al. Glioblastoma stem cells exploit the alphavbeta8 integrin-TGFbeta1 signaling axis to drive tumor initiation and progression. Oncogene 2017; 36: 6568–6580. [PubMed: 28783169]
21. Reyes SB, Narayanan AS, Lee HS, Tchaicha JH, Aldape KD, Lang FF et al. alphavbeta8 integrin interacts with RhoGDI1 to regulate Rac1 and Cdc42 activation and drive glioblastoma cell invasion. Mol Biol Cell 2013; 24: 474–482. [PubMed: 23283986]
22. Chen Z, Morales JE, Guerrero PA, Sun H, McCarty JH. PTPN12/PTP-PEST Regulates Phosphorylation-Dependent Ubiquitination and Stability of Focal Adhesion Substrates in Invasive Glioblastoma Cells. Cancer Res 2018; 78: 3809–3822. [PubMed: 29743287]

23. Dundar B, Markwell SM, Sharma NV, Olson CL, Mukherjee S, Brat DJ. Methods for in vitro modeling of glioma invasion: Choosing tools to meet the need. Glia 2020.
24. Hoegg-Beiler MB, Sirisi S, Orozco IJ, Ferrer I, Hohensee S, Auberson M et al. Disrupting MLC1 and GlialCAM and ClC-2 interactions in leukodystrophy entails glial chloride channel dysfunction. Nat Commun 2014; 5: 3475. [PubMed: 24647135]
25. Hwang J, Vu HM, Kim MS, Lim HH. Plasma membrane localization of MLC1 regulates cellular morphology and motility. Mol Brain 2019; 12: 116. [PubMed: 31888684]
26. Brignone MS, Lanciotti A, Macioce P, Macchia G, Gaetani M, Aloisi F et al. The beta1 subunit of the Na,K-ATPase pump interacts with megalencephalic leucoencephalopathy with subcortical cysts protein 1 (MLC1) in brain astrocytes: new insights into MLC pathogenesis. Human molecular genetics 2011; 20: 90–103. [PubMed: 20926452]
27. Leegwater PA, Boor PK, Yuan BQ, van der Steen J, Visser A, Konst AA et al. Identification of novel mutations in MLC1 responsible for megalencephalic leukoencephalopathy with subcortical cysts. Human genetics 2002; 110: 279–283. [PubMed: 11935341]
28. Leegwater PA, Yuan BQ, van der Steen J, Mulders J, Konst AA, Boor PK et al. Mutations of MLC1 (KIAA0027), encoding a putative membrane protein, cause megalencephalic leukoencephalopathy with subcortical cysts. American journal of human genetics 2001; 68: 831–838. [PubMed: 11254442]
29. van der Knaap MS, Lai V, Kohler W, Salih MA, Fonseca MJ, Benke TA et al. Megalencephalic leukoencephalopathy with cysts without MLC1 defect. Annals of neurology 2010; 67: 834–837. [PubMed: 20517947]
30. Nishizuka SS, Mills GB. New era of integrated cancer biomarker discovery using reverse-phase protein arrays. Drug Metab Pharmacokinet 2016; 31: 35–45. [PubMed: 26822993]
31. Lewis-Tuffin LJ, Feathers R, Hari P, Durand N, Li Z, Rodriguez FJ et al. Src family kinases differentially influence glioma growth and motility. Mol Oncol 2015; 9: 1783–1798. [PubMed: 26105207]
32. Ma W, Na M, Tang C, Wang H, Lin Z. Overexpression of N-myc downstream-regulated gene 1 inhibits human glioma proliferation and invasion via phosphoinositide 3-kinase/AKT pathways. Mol Med Rep 2015; 12: 1050–1058. [PubMed: 25777142]
33. Hara A, Kanayama T, Noguchi K, Niwa A, Miyai M, Kawaguchi M et al. Treatment Strategies Based on Histological Targets against Invasive and Resistant Glioblastoma. J Oncol 2019; 2019: 2964783. [PubMed: 31320900]
34. Peglion F, Goehring NW. Switching states: dynamic remodelling of polarity complexes as a toolkit for cell polarization. Curr Opin Cell Biol 2019; 60: 121–130. [PubMed: 31295650]
35. Onken J, Vajkoczy P, Torka R, Hempt C, Patsouris V, Heppner FL et al. Phospho-AXL is widely expressed in glioblastoma and associated with significant shorter overall survival. Oncotarget 2017; 8: 50403–50414. [PubMed: 28881571]
36. Sadahiro H, Kang KD, Gibson JT, Minata M, Yu H, Shi J et al. Activation of the Receptor Tyrosine Kinase AXL Regulates the Immune Microenvironment in Glioblastoma. Cancer Res 2018; 78: 3002–3013. [PubMed: 29531161]
37. Antony J, Huang RY. AXL-Driven EMT State as a Targetable Conduit in Cancer. Cancer Res 2017; 77: 3725–3732. [PubMed: 28667075]
38. Rao L, Mak VCY, Zhou Y, Zhang D, Li X, Fung CCY et al. p85beta regulates autophagic degradation of AXL to activate oncogenic signaling. Nat Commun 2020; 11: 2291. [PubMed: 32385243]
39. Lanciotti A, Brignone MS, Visentin S, De Nuccio C, Catacuzzeno L, Mallozzi C et al. Megalencephalic leukoencephalopathy with subcortical cysts protein-1 regulates epidermal growth factor receptor signaling in astrocytes. Hum Mol Genet 2016; 25: 1543–1558. [PubMed: 26908604]
40. Leventoux N, Augustus M, Azar S, Riquier S, Villemin JP, Guelfi S et al. Transformation Foci in IDH1-mutated Gliomas Show STAT3 Phosphorylation and Downregulate the Metabolic Enzyme ETNPPL, a Negative Regulator of Glioma Growth. Sci Rep 2020; 10: 5504. [PubMed: 32218467]

41. Antony J, Tan TZ, Kelly Z, Low J, Choolani M, Recchi C et al. The GAS6-AXL signaling network is a mesenchymal (Mes) molecular subtype-specific therapeutic target for ovarian cancer. Sci Signal 2016; 9: ra97. [PubMed: 27703030]

42. Lanciotti A, Brignone MS, Belfiore M, Columba-Cabezas S, Mallozzi C, Vincentini O et al. Megalencephalic Leukoencephalopathy with Subcortical Cysts Disease-Linked MLC1 Protein Favors Gap-Junction Intercellular Communication by Regulating Connexin 43 Trafficking in Astrocytes. Cells 2020; 9.

43. Brignone MS, Lanciotti A, Camerini S, De Nuccio C, Petrucci TC, Visentin S et al. MLC1 protein: a likely link between leukodystrophies and brain channelopathies. Frontiers in cellular neuroscience 2015; 9: 66.

44. Turner KL, Sontheimer H. Cl- and K+ channels and their role in primary brain tumour biology. Philos Trans R Soc Lond B Biol Sci 2014; 369: 20130095. [PubMed: 24493743]

45. Gaitan-Penas H, Apaja PM, Arnedo T, Castellanos A, Elorza-Vidal X, Soto D et al. Leukoencephalopathy-causing CLCN2 mutations are associated with impaired Cl(−) channel function and trafficking. J Physiol 2017; 595: 6993–7008. [PubMed: 28905383]

46. McCarty JH. alphavbeta8 integrin adhesion and signaling pathways in development, physiology and disease. J Cell Sci 2020; 133.

47. Elorza-Vidal X, Xicoy-Espaulella E, Pla-Casillanis A, Alonso-Gardon M, Gaitan-Penas H, Engel-Pizcueta C et al. Structural basis for the dominant or recessive character of GLIALCAM mutations found in leukodystrophies. Hum Mol Genet 2020; 29: 1107–1120. [PubMed: 31960914]

48. Amiry-Moghaddam M, Ottersen OP. The molecular basis of water transport in the brain. Nat Rev Neurosci 2003; 4: 991–1001. [PubMed: 14682361]

49. Waite A, Brown SC, Blake DJ. The dystrophin-glycoprotein complex in brain development and disease. Trends Neurosci 2012; 35: 487–496. [PubMed: 22626542]

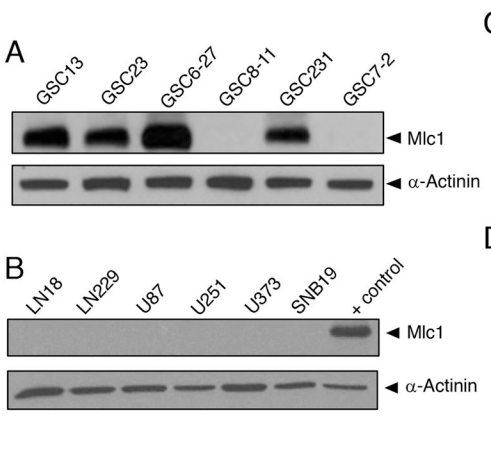

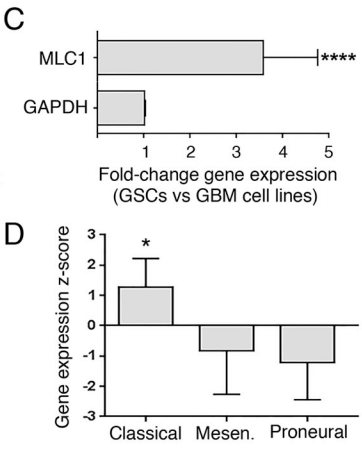

E

Correlated Gene	Pearson's Correlation	Spearman's Correlation
HEPACAM	0.61	0.71
LRRC16A	0.69	0.70
BBOX1	0.62	0.70
SIPAIL1	0.62	0.70
MCC	0.67	0.68
PIPOX	0.58	0.68
ABHD17C	0.55	0.68
AQP4	0.60	0.68
HEPN1	0.56	0.67
CERS1	0.64	0.67
ATP1B2	0.63	0.67
IVD	0.60	0.66
GAS2L1	0.58	0.66
DTNA	0.60	0.66
ITGB8	0.51	0.65

Figure 1. MLC1 is expressed in primary human GSCs.

(A); Detergent-soluble lysates from six different primary human GSC spheroid cultures were immunoblotted with anti-Mlc1 antibodies. Note the robust expression of Mlc1 protein in four of the GSC samples. **(B);** Immunoblotting detergent-soluble lysates from six different human GBM cell lines reveals lack of detectable Mlc1 protein expression. As positive controls (+ controls) for these immunoblots, lysates from transfected HEK-293T cells expressing exogenous Mlc1 protein were used. **(C);** Quantitation of MLC1 mRNA levels reveals enrichment in human GSCs versus several established human GBM cell lines. These data were mined from the cBioPortal genomic database. The z-score for MLC1 mRNA levels was 1.2 standard deviations greater in the classical GBM subtype versus non-cancerous brain tissue samples, ***$p<0.001$. **(D);** MLC1 expression is enriched in the classical GBM sub-type, as determined by analysis of mRNA levels in the TCGA database, *$p<0.05$. Differences between groups were analyzed using two-way analysis of variance (ANOVA) with Bonferroni post-hoc test. **(E);** Analysis of the cBioPortal genomic database reveals that expression of MLC1 mRNA is most correlative with HEPACAM/GLIALCAM expression in human tumor specimens. Several other genes also show coincident expression, including ITGB8 which like MLC1 is a molecular marker for the classical GBM sub-type.

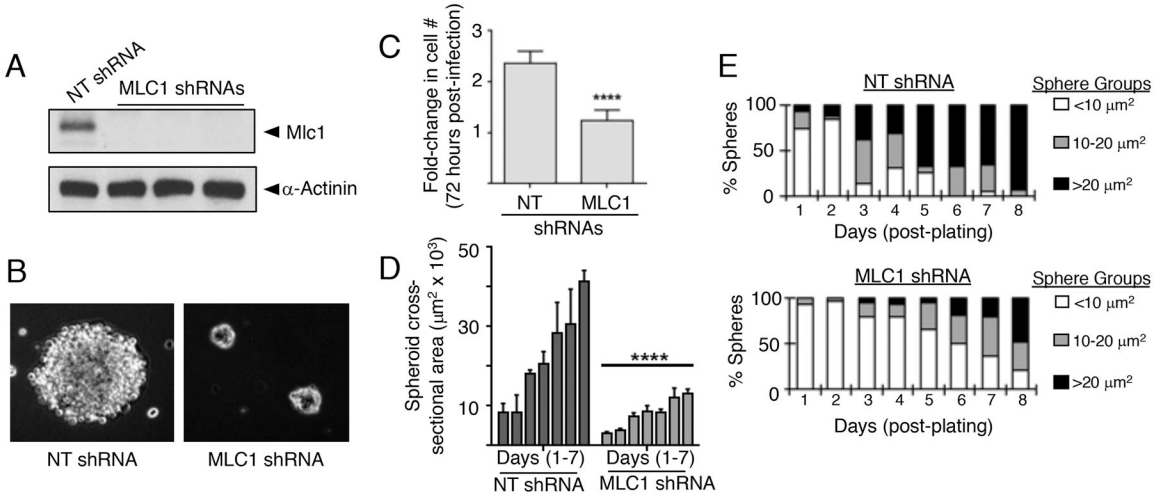

Figure 2. MLC1 promotes GSC spheroid formation in vitro.

(A); pGIPZ lentivirus-expressed shRNAs were tested for MLC1 (n=3) gene silencing in infected GSC6–27 cells. All three MLC1 shRNAs silenced gene expression by >90% as determined by anti-Mlc1 immunoblotting. As negative controls for these experiments we used GSC6–27 cells infected with pGIPZ lentivirus expressing non-targeting (NT) shRNAs. **(B);** GSC6–27 cells infected with control pGIPZ lentivirus formed neurosphere-like spheroids that were significantly larger than spheroids formed from cells expressing MLC1 shRNAs. **(C);** At 72 hours post-lentivirus infection, GSC6–27 cells expressing MLC1 shRNAs showed a significant reduction in total cell number in comparison to GSC6–27 cells expressing control shRNAs, ***p<0.001. **(D);** Single cell suspensions were allowed to form spheroids over 7 days. The cross-sectional area of newly formed spheroids was recorded each day, revealing MLC1-dependent defects in spheroid sizes, *p<0.05 and ***p<0.001. Differences between groups were analyzed using two-way ANOVA with Bonferroni post-hoc test. **(E);** The cross-sectional areas of spheroids were recorded daily for 8 consecutive days. GSC6–27 cells expressing MLC1 shRNAs formed spheroids that were significantly smaller in comparison to GSC6–27 cells expressing control non-targeting (NT) shRNAs. The percentages of total spheroids with measured cross-sectional areas (grouped as <10 μm^2, 10–20 μm^2, or >20 μm^2). are shown on the y-axes. The days (1–8) on which the sphere cross-sectional areas were measured are indicated on the x-axis.

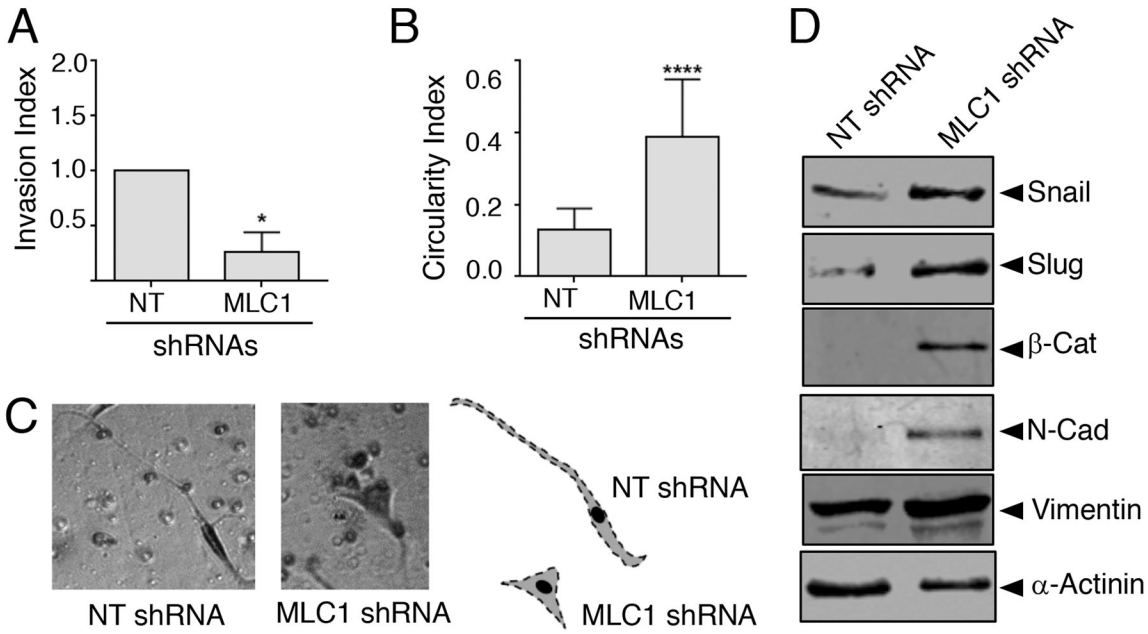

Figure 3. MLC1 promotes GSC polarity and invasion in vitro.

(A); GSC6–27 cells expressing MLC1 shRNAs showed diminished invasion through the Matrigel-coated transwells as compared to control pGIPZ-infected cells, *p<0.05. **(B);** MLC1 regulates the polarity and mesenchymal-like features of cells that have invaded through the Matrigel-coated transwells as determined by analyzing cell shapes, ***p<0.001. Differences between groups (in A, B) were analyzed using two-way ANOVA with Bonferroni post-hoc test. **(C);** The outlines of hematoxylin-stained GSC6–27 cells expressing non-targeting shRNAs or MLC1 shRNAs that invaded through the Matrigel-coated transwell were traced. Note that GSC6–27 cells expressing MLC1 shRNAs were more epithelial-like, whereas GSC6–27 cells expressing control shRNAs were more elongated and displayed mesenchymal-like shapes. Representative GSC6–27 cell tracings are show in the images on the right. **(D);** Expression of various proteins with links to cell polarity and the epithelial to mesenchymal transition were analyzed in GSC6–27 cells expressing NT shRNAs or MLC1 shRNAs by immunoblotting detergent-soluble lysates.

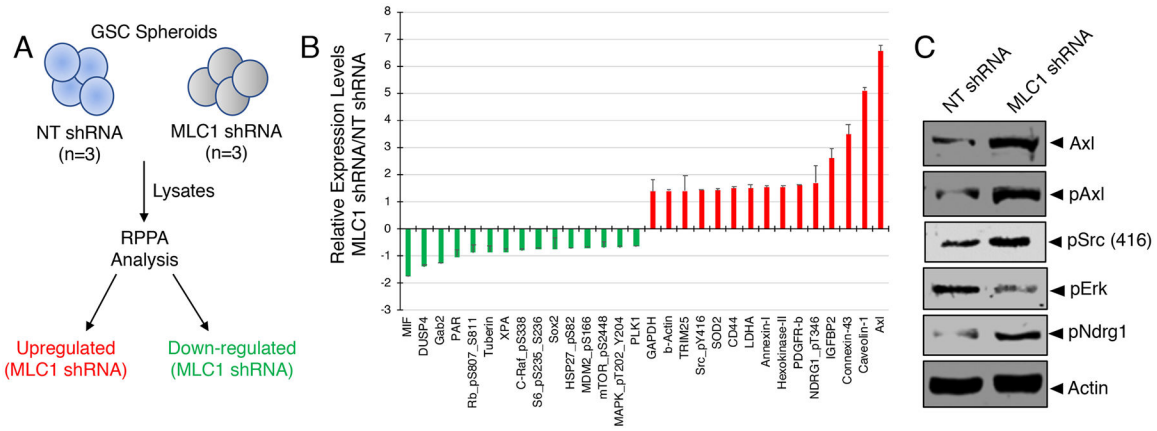

Figure 4. RPPA analysis of MLC1-regulated signaling pathways in GSCs.

(A); Strategy to identify MLC1-dependent changes in protein expression or phosphorylation in cancer cells using RPPA, a high-throughput antibody platform. **(B);** Bar graph summarizing select proteins that show statistically significant differences in expression and/or phosphorylation in GBM cells expressing MLC1 shRNAs versus control cells. Shown are the top 15 proteins displaying reduced (green) or elevated (red) expression and/or phosphorylation in MLC1 shRNA cells versus NT shRNA cells. **(C);** Immunoblots of detergent-soluble lysates from GSC6–27 cells expressing MLC1 shRNAs versus control NT shRNAs reveals differential expression and/or phosphorylation of select proteins identified by RPPA.

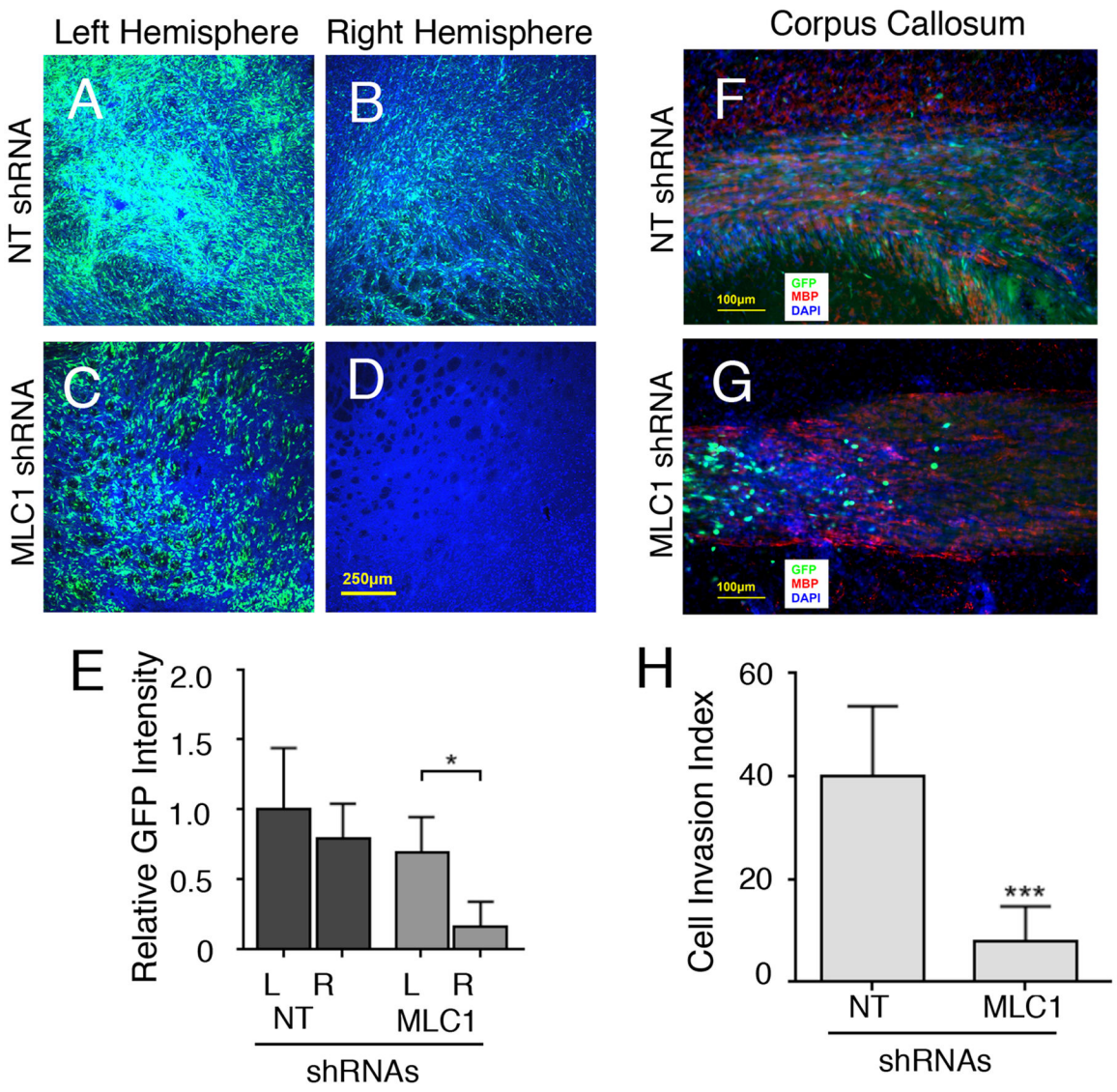

Figure 5. MLC1 promotes GSC invasive growth in the brain microenvironment

(A-D); Coronal sections through the striatum of mice harboring tumors formed from GSC6–27 cells expressing control non-targeting (NT) shRNAs (A, B) or MLC1 shRNAs (C, D) were immunofluorescently labeled with anti-GFP antibodies to identify GBM cells. Shown are images of the injected left hemisphere (A, C) and the non-injected right hemisphere (B, D). Note that tumors derived from GSC6–27 cells expressing non-targeting shRNAs showed cell invasion from the injection site (A) into the opposite hemisphere (B). In contrast, GSC6–27 cells expressing MLC1 shRNAs formed tumors (C) but were defective in invasion to the opposing hemisphere (D). **(E);** Quantitative results showing that MLC1 expression is required for the ability of GSC6–27 cells to invade from the injected striatum (L) to the opposite brain hemisphere (R), *p<0.05. **(F, G);** Invasive GBM cells (green) traversed across myelin basic protein (MBP)-positive white matter tracts (red) that comprise the corpus callosum. Note that GSC6–27 cells expressing control shRNAs (F) showed robust invasion in the corpus callosum, whereas GBM cells expressing MLC1 shRNAs (G) showed

diminished invasion through the corpus callosum. **(H);** Quantitation of GSC6–27 cell invasion in the corpus callosum, revealing MLC1-dependent defects in white matter invasion in comparison to GSC6–27 cells expressing control shRNAs, ***$p<0.001$. Differences between NT shRNA and MLC1 shRNA groups were analyzed using two-way ANOVA with Bonferroni post-hoc test.

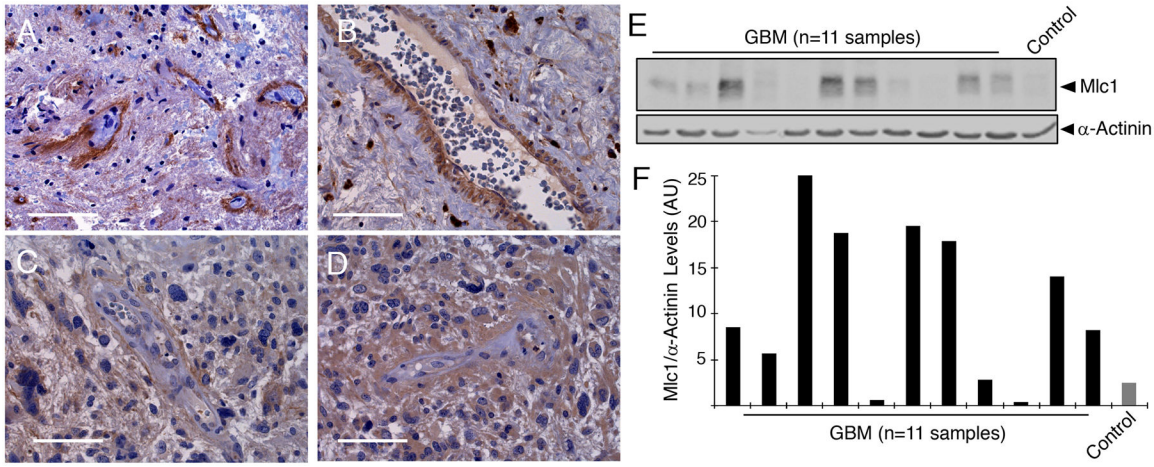

Figure 6. Analysis of Mlc1 protein expression in human GBM tissue samples.

(A-D); Analysis of four different fixed human GBM tissue sections by anti-Mlc1 immunohistochemistry showed that Mlc1 protein was expressed in GBM cells throughout the tumor. Note that there is some enriched expression of Mlc1 protein mainly at contact points with cerebral blood vessels. Scale bars, 30 μm. **(E);** A panel of detergent-soluble lysates from human GBM tissues (n=11) were analyzed by anti-Mlc1 immunoblotting. Note that many GBM samples express Mlc1 protein. The control lane contains a sample of non-cancerous human brain tissue lysate. **(F);** Quantitation of Mlc1 protein expression in GBM tissue lysates based on densitometry analysis of the immunoblot data in (E), normalized to the α-actinin loading control.

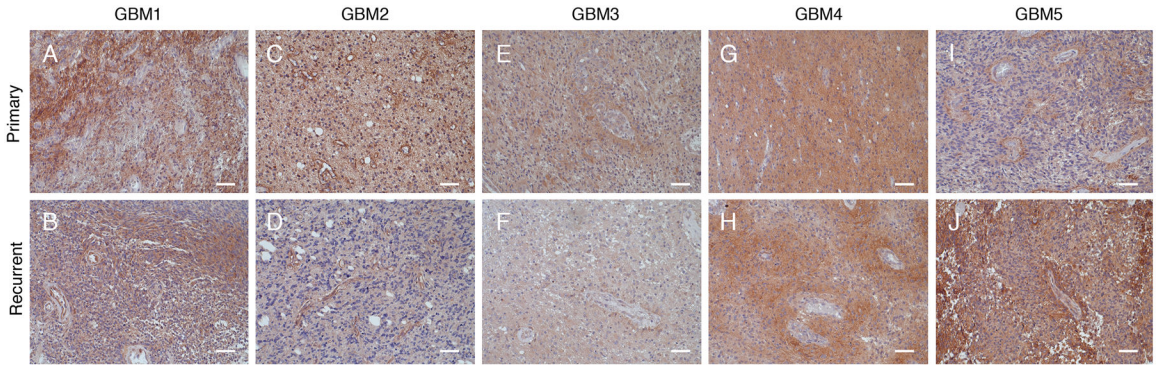

Figure 7. Analysis of Mlc1 protein expression in primary and recurrent human GBM samples.

(A-J); Anti-Mlc1 immunohistochemical staining of matched primary (A, C, E, G, I) and recurrent (B, D, F, H, J) GBM tissue samples resected from five different patients. Primary tumors were resected prior to therapy, whereas tumor that recurred were resected after standard chemotherapy and radiation. Note that Mlc1 protein is expressed in cancer cells in all 5 primary GBM samples and expression levels are maintained or elevated in matched recurrent GBM samples. These results support important roles for Mlc1 in invasive GSCs, which escape surgical resection and generate recurrent lesions after chemoradiation. Scale bars, 50 μm.

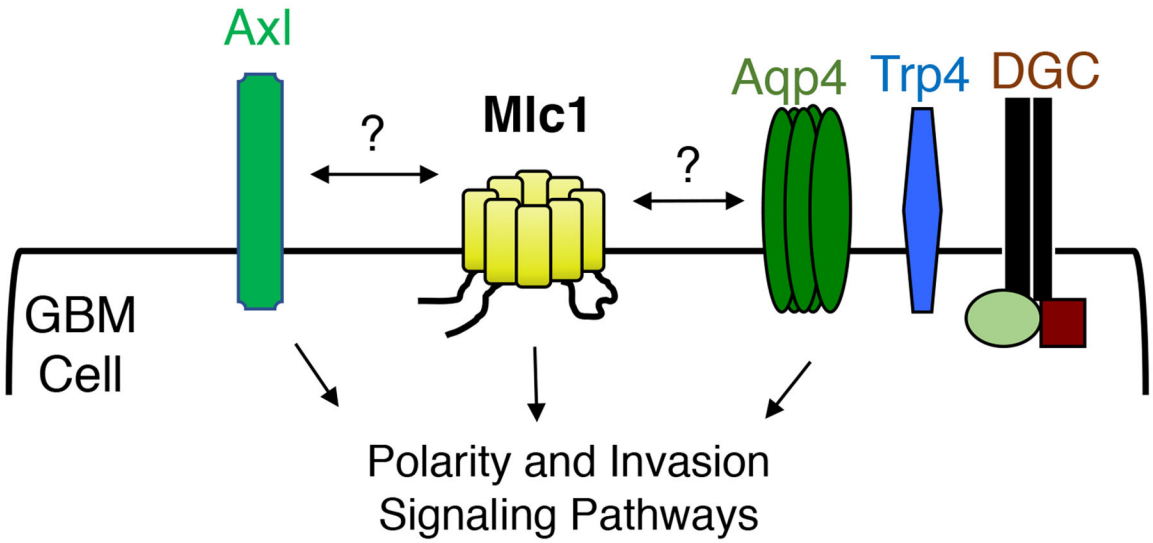

Figure 8. A model for Mlc1 control of GBM cell polarity and invasive growth in the brain microenvironment.

Mlc1 protein is expressed in GBM cells, where it regulates contact and communication with stromal components in the brain microenvironment to activate pro-invasive signaling pathways. Mlc1-dependent regulation of Axl at the cell surface and its various intracellular signaling proteins drive invasion. Inhibiting Mlc1 functions in GBM cells leads to impaired cell polarity and diminished invasive growth. We propose that Mlc1 interacts with other cell surface proteins including GlialCAM, Aqp4, Trp4, and components of the DGC to modulate the microenvironment and activate signaling pathways that promote GSC invasion.